

Bitcoin Volatility and Intrinsic Time Using Double Subordinated Lévy Processes

Abootaleb Shirvani* Stefan Mittnik† W. Brent Lindquist‡
Svetlozar Rachev§

Abstract

We propose a doubly subordinated Levy process, NDIG, to model the time series properties of the cryptocurrency bitcoin. NDIG captures the skew and fat-tailed properties of bitcoin prices and gives rise to an arbitrage free, option pricing model. In this framework we derive two bitcoin volatility measures. The first combines NDIG option pricing with the Cboe VIX model to compute an implied volatility; the second uses the volatility of the unit time increment of the NDIG model. Both are compared to a volatility based upon historical standard deviation. With appropriate linear scaling, the NDIG process perfectly captures observed, in-sample, volatility.

(*JEL*: C02, G12, G13)

Keywords: bitcoin volatility; subordinated Lévy processes; intrinsic time

*Department of Mathematical Science, Kean University, ashirvan@kean.edu.

†Department of Statistics, Ludwig Maximilians University, mittnik@gmx.de.

‡Department of Mathematics & Statistics, Texas Tech University, brent.lindquist@ttu.edu.

§Department of Mathematics & Statistics, Texas Tech University, zari.rachev@ttu.edu.

1 Introduction

Cryptocurrencies have emerged as an alternative asset class in their own right. By now, institutional as well as private investors have taken a closer look at this asset class. Many view digital currencies, particularly the leading cryptocurrency, bitcoin, as an alternative to gold for providing long-term protection against inflation. In contrast, a major argument against investing in cryptocurrencies is their high and often erratic volatility when compared to conventional speculative assets.

Data on bitcoin volatility, in terms of the Bitcoin Volatility Index (BVI), have been available since 2010.¹ The BVI index is based on historical volatility, specifically, the standard deviation of past daily log-returns. Two versions of this index are provided, based on 30- and 60-day windows of past observations. The problem with historical volatility is that it is only meaningful if the returns are approximately independent and identically distributed (iid). In the presence of temporal dependence in the form of volatility clustering, a phenomenon common to virtually all speculative assets, including cryptocurrencies, historical volatility fails to adequately capture the current risk of an investment in a speculative asset. It simply provides an average of past risk.

Implied volatility measures attempt to tackle this shortcoming by capturing the current market view on future risk as implied by observed transaction prices of option contracts. Assuming an option-pricing method and given the price at which an option has been traded, one can back out the expected volatility of the underlying asset that is implied by the observed price. Several approaches have been developed to price options contracts, including continuum models such as the Black and Scholes (1973) and Merton (1973) (BSM) formula, as well as discrete models based on binomial or trinomial trees, Monte Carlo simulation, discrete stochastic volatility, and finite-differencing methods.

Alexander and Imeraj (2021) use bitcoin options data from the Deribit exchange to create a term structure for bitcoin implied volatility indices using the same variance swap fair-value formula (geometric variance swap) that the Chicago Board Options Exchange (Cboe) uses to construct the VIX index (CBOE, 2019) that reflects the volatility of the S&P 500 stock index. Furthermore, Alexander and Imeraj point out that bitcoin prices appear to fluctuate excessively, so that this approach tends to underestimate the fair value of geometric variance swaps. In a recent report, Kim et al. (2019) proposed a volatility index based on the cryptocurrency index CRIX.² It proxies the next month's mean annualized volatility. Venter and Maré (2020) used the symmetric GARCH option pricing model to construct various implied volatility indices, including the CRIX index. More recently, an alternative volatility index, BitVol (T3I-Pty-Ltd., 2019), has been introduced. It reflects the expected 30-day implied volatility derived from tradable bitcoin option prices using the BSM model.

The BSM model rests upon the assumption that the returns of the underlying asset follow a normal distribution. There is, however, overwhelming empirical evidence that return distributions exhibit heavy tails and asymmetry. Osterrieder (2016) demonstrated that these properties hold for bitcoin returns. The omnipresence of extreme return observations indicates that a heavy-tailed distribution should provide a more realistic description for the

behavior of bitcoin returns. Heavy tails and asymmetry contradict the normality assumption and present a challenge to BSM option pricing. The Student’s t -distribution would be an obvious candidate for heavy-tailed data. However, in the context of option pricing, use of the t -distribution in the BSM setting results in a divergent integral (Cassidy et al., 2010). Recently, Näf et al. (2019) proposed a mean–variance heterogeneous tails mixture distribution for modeling financial asset returns. They showed that the new model captures, along with the obligatory leptokurtosis, different tail behavior among the assets.

The method of subordination³ offers an alternative approach to addressing non-normality. By adopting the concept of intrinsic or operational time rather than calendar time, the method of subordination allows the variance of the normal distribution to change over time and to capture heavy-tailed phenomena. The subordination approach leads to a generalization of the classical asset pricing model.⁴ Shirvani et al. (2021) introduced and analyzed various *multiple* subordination processes and demonstrated that the resulting dynamics lead to more realistic asset pricing models. The idea of multiple subordination is motivated both by the need to better capture the heavy-tailedness that conventional Lévy-subordinated models fail to explain and the desire to incorporate the views of investors in asset and option pricing models.

In this paper, we develop a bitcoin volatility index based on the Cboe variance swap fair-value formula but with log-prices following a double subordinated process. We briefly introduce the idea of double subordination to model the dynamics of Lévy processes. We show our model implies a heavy-tailed distribution that provides a better description of bitcoin log-prices than the Student’s t model.

Rather than using Monte Carlo option pricing in non-Gaussian settings, as put forth in Allen et al. (2011), we employ the arbitrage theorem and mean-correction martingale measure (MCMM) of Yao et al. (2011) to price options when the returns of the underlying assets are doubly subordinated. Specifically, we price European contingent claims when bitcoin returns are assumed to be driven by a double subordinated Lévy process. We determine the equivalent martingale measure to price options using the MCMM approach and demonstrate that our proposed pricing model is arbitrage free. Based on generated bitcoin option data, we derive implied volatilities using the Cboe approach and the double subordination approach.

The remainder of the paper is organized as follows. Section 2 describes the double subordinated process and applies it to model bitcoin log-prices. Section 3 details the option pricing framework under double subordination and applies it to model bitcoin vanilla European call and put options. In Section 5 we assess bitcoin volatility using the Cboe approach, which is based upon option pricing, and our intrinsic time approach based upon spot pricing. Both methods are compared with historical volatility. The paper concludes with a discussion of our results.

2 Double Subordination Model for Bitcoin Log-Prices

The double subordination framework adopted here involves a Lévy subordinator process. A stochastic process $\mathbb{X} = (X(t), t \geq 0)$ defined on a stochastic basis $(\Omega, \mathcal{F}, \mathbb{F}, \mathbb{P})$ is said to be a *Lévy process* if the following conditions hold.

- $X(0) = 0$, \mathbb{P} -almost surely.
- \mathbb{X} is a process with independent increments; for any partition $0 = t_0 < t_1 < \dots < t_n < \infty$, the increments $X(t_i) - X(t_{i-1})$, $i = 1, 2, \dots, n$ are independent.
- \mathbb{X} is a process with stationary increments; for any $0 \leq s < t$, the increment $X(t) - X(s)$ has the same distribution as $X(t - s)$, that is, $X(t) - X(s) \sim X(t - s)$.⁵
- \mathbb{X} is continuous in probability; for every $\varepsilon > 0$ and $t \geq 0$, there exists $h_{\varepsilon, t} > 0$, such that $\mathbb{P}(|X(t + h_{\varepsilon, t}) - X(t)| > \varepsilon) < \varepsilon$.

In dynamic asset-pricing theory, a risky financial asset is defined by its price dynamics S_t , $t \in [0, \tau]$, where $\tau < \infty$ is the time horizon; that is, τ is the maturity date of a financial contract. A Lévy process $\mathbb{T} = (T(t), t \geq 0, T(0) = 0)$ with non-decreasing trajectories (i.e., non-decreasing sample paths) is called a *Lévy subordinator*. Since $T(0) = 0$, the trajectories of \mathbb{T} take only non-negative values. In the BSM option pricing model, the price dynamics of the underlying asset are defined by

$$S_t^{(\text{BSM})} = e^{X_t^{(\text{BSM})}}, \quad t \in [0, \tau], \quad (1)$$

where the log-process is

$$X_t^{(\text{BSM})} = X_0 + \mu_1 t + \sigma_1 B_t, \quad \mu_1 \in R, \sigma_1 > 0, X_0 = \ln(S_0), S_0 > 0, \quad (2)$$

and $\mathbb{B} = (B_t, t \geq 0)$ is a standard Brownian motion. To allow for non-normality of asset returns, Mandelbrot and Taylor (1967) and Clark (1973) suggested the use of a subordinated Brownian motion, where the price process $S_t^{(\text{ss})}$ and the log-price process are defined as

$$S_t^{(\text{ss})} = e^{X_t^{(\text{ss})}}, \quad t \in [0, \tau], \quad (3)$$

$$X_t^{(\text{ss})} = X_0 + \mu_2 t + \sigma_2 B_{T(t)}, \quad \mu_2 \in R, \sigma_2 > 0, \quad (4)$$

where $\mathbb{T} = (T(t), t \geq 0, T(0) = 0)$ is a Lévy subordinator.

Process (4) describes the well-known *single* subordinated log-price process. Various studies have demonstrated that single subordinated log-price models commonly fail to capture the heavy-tailedness observed in financial return data. For example, Lundtofte and Wilhelmsson (2013) and Shirvani et al. (2021) showed that the normal-inverse Gaussian (NIG) distribution, which is a single subordinated Lévy process, fails to explain the equity premium puzzle. This is partly due to the fact that the tails produced by NIG are not heavy enough. However, Shirvani et al. (2021) demonstrated that the high value for the

risk aversion coefficient, which gives rise to the equity premium puzzle, is compatible with a return process driven by a double subordinator model. Shirvani et al. (2021) defined and investigated the properties of various multiple subordinated log–return processes designed to model leptokurtic asset returns. They showed that multiple subordinated log–return processes can imply heavier tails than single subordinated models and that they are capable of capturing skewness and kurtosis. Therefore, a double subordination framework may be a more appropriate candidate for modeling the rather extreme behavior of bitcoin.

To apply double subordination to modeling the bitcoin price process, let S_t denote the price process with the dynamics

$$S_t = e^{X_t}, \quad t \in [0, \tau], \quad (5)$$

$$X_t = X_0 + \mu_3 t + \gamma U(t) + \rho T(U(t)) + \sigma_3 B_{T(U(t))}, \quad t \geq 0, \mu_3 \in \mathbb{R}, \sigma_3 > 0, X_0 = \ln(S_0), S_0 > 0, \quad (6)$$

where the triplet members $\{B_s, T(s), U(s)\}, s \geq 0$, are independent processes generating the stochastic basis $(\Omega, \mathcal{F}, \mathbb{F} = (\mathcal{F}_t, t \geq 0), \mathbb{P})$ representing the real world. Here, $\{B_s, s \geq 0\}$ is a standard Brownian motion, while $\{T(s), s \geq 0, T(0) = 0\}$ and $\{U(s), s \geq 0, U(0) = 0\}$ are Lévy subordinators. $B_t, T(t)$ and $U(t)$ are \mathcal{F}_t -adapted processes, whose trajectories are right-continuous with left limits. Shirvani et al. (2021) referred to $T(U(t)), t \geq 0$ as the *double subordinator process*; hence, the process modeled by (6) is a *double subordinated log–price process*.

Consider the case where the subordinators $T(t)$ and $U(t)$ are inverse Gaussian (IG) Lévy processes; that is, $T(1) \sim IG(\lambda_T, \mu_T)$ having the probability density function (pdf),

$$f_{T(1)}(x) = \sqrt{\frac{\lambda_T}{2\pi x^3}} \exp\left(-\frac{\lambda_T(x - \mu_T)^2}{2\mu_T^2 x}\right), \quad x \geq 0, \lambda_T > 0, \mu_T > 0. \quad (7)$$

Similarly $U(1) \sim IG(\lambda_U, \mu_U)$. In this case, Shirvani et al. (2021) referred to $T(U(t))$ as the *double inverse Gaussian subordinator* and to X_t as a *normal double inverse Gaussian (NDIG) log–price process*. The characteristic function (chf) of X_1 is given by

$$\varphi_{X_1}(v) = \mathbb{E}[e^{ivX_1}] = \exp\left\{iv\mu_3 + \frac{\lambda_U}{\mu_U} \left[1 - \sqrt{1 - \frac{2\mu_U^2}{\lambda_U} \left(\frac{\lambda_T}{\mu_T} \left(1 - \sqrt{1 - \frac{\mu_T^2}{\lambda_T} (2iv\rho - \sigma_3^2 v^2)}\right) + iv\lambda\right)}\right]\right\}, \quad (8)$$

with $v \in \mathbb{R}$. The moment generating function (MGF) of X_1 is $M_{X_1}(w) = \mathbb{E}[e^{wX_1}]$, $w \in \mathbb{R}$.

The NDIG model 6 and 8 has eight parameters, namely $\mu_3, \sigma_3, \gamma, \rho, \mu_\tau, \lambda_\tau, \mu_T$ and λ_T , which can make fitting the model to data a challenging task. However, it is worth noting that that only six of these parameters are identifiable within the model.¹ To set the remaining two parameters, we can consider the expectation:

¹See Lindquist et al. (2022).

$$\mathbb{E}[X_1] = \mu_3 + \gamma\mathbb{E}[U(1)] + \rho\mathbb{E}[X(v)]\mathbb{E}[T(U(1))] \quad (9)$$

As the processes U and T are independent inverse Gaussian (IG) processes, we can uniquely identify γ and ρ by requiring:

$$\mathbb{E}[U(1)] = \mu_U = 1 \quad \text{and} \quad \mathbb{E}[T(U(1))] = \mu_U\mu_T = 1 \quad \rightarrow \quad \mu_T = 1. \quad (10)$$

By utilizing equation 10, the set of model parameters that can be identified becomes μ_3 , σ_3 , γ , ρ , λ_T , and λ_U .

The central moments of the NDIG can serve as a source of data for fitting these six parameters. The moment generating function (MGF) $M_{X_1}(w)$ for X_1 , which generates the moments of its probability distribution, can be obtained by evaluating $\mathbb{E}[e^{iwX_1}]$ for $w \in \mathbb{R}$. This can be obtained from equation 8 by setting $w = iv$. The MGF is written in terms of the cumulant generating function $K(w)$:

$$M_{X_1}(w) = \mathbb{E}[e^{iwX_1}] = \exp(K_{X_1}(w)). \quad (11)$$

Using the identity

$$\varphi_{X_t}(v) = \mathbb{E}[e^{ivX_t}] = (\mathbb{E}[e^{ivX_1}])^t = [\varphi(X_1)]^t, \quad (12)$$

we can express $M_{X_t}(w)$ as $M_{X_t}(w) = \exp(K_{X_1}(w)t)$, where $K_{X_1}(w)$ can be written using equation 11 as:

$$\begin{aligned} K_{X_1}(w) &= \mu_3 w + \lambda_U \left(1 - \sqrt{1 - g(w)}\right), \\ g(w) &= 1 - 2\frac{\lambda_T}{\lambda_U} \left(1 - \sqrt{h(w)}\right) - 2\frac{\gamma}{\lambda_U} w, \\ h(w) &= 1 - \frac{2\rho w}{\lambda_T} - \frac{\sigma_3^2 w^2}{\lambda_T}. \end{aligned} \quad (13)$$

Now, by finding the first four central derivatives of $K_{X_1}(w)$, we can have the first four centered moments of X_1 .

$$\begin{aligned} E[X] &= \mu_3 + s, \\ Var[X] &= \sigma + \frac{s^2}{\lambda_U}, \\ Skew[X] &= \frac{3\left(\sigma c + \frac{s^3}{\lambda_U^2}\right)}{\left(\sigma + \frac{s^2}{\lambda_U}\right)^{3/2}}, \\ Kurt[X] &= 3\frac{[\sigma^2(1/\lambda_T + 1/\lambda_U) + 2\sigma(c^2 + (\rho/\lambda_T)^2 + 2(s/\lambda_U)^2) + 5s^4/\lambda_U^3]}{\left(\sigma + \frac{s^2}{\lambda_U}\right)^2}, \end{aligned} \quad (14)$$

where $s = \gamma + \rho$, $\sigma = \rho^2/\lambda_T + \sigma_3^2$, and $c = \rho/\lambda_T + s/\lambda_U$. Equation 32 presents four criteria for fitting the six model parameters. The subsequent section on numerical computation will discuss additional requirements for parameter estimation.

3 Bitcoin Option Pricing under Double Subordination

To price European contingent claims, we assume that X_t follows a NDIG log-price process. We need to derive an equivalent martingale measure (EMM) \mathbb{Q} of \mathbb{P} on $(\Omega, \mathcal{F}, \mathbb{F} = (\mathcal{F}_t, t \geq 0), \mathbb{P})$, such that the discounted price process, $e^{-rt}S_t$ with $r \geq 0$ denoting the riskless rate, is a martingale.⁷ To do so, we use the MCMM, since the proposed pricing model is arbitrage-free under MCMM, and estimate the parameters specifying the process. We then add the appropriate drift term to the process, such that the discounted price process becomes a martingale.

Yao et al. (2011) constructed a martingale measure using MCMM for the geometric Lévy process model and showed that this measure is an EMM if there is a continuous Gaussian part in the Lévy process. In the case that X_t is a pure jump Lévy process, they pointed out that this measure cannot be equivalent to a physical probability. However, pricing European options under this measure is still arbitrage free.

Let \mathcal{C} be a European call option having an underlying risky asset \mathcal{S} with a price and log-price process as in (5) and (6), respectively. Let \mathcal{B} be a riskless asset with price $b_t = e^{rt}$, $t \geq 0$, where $r \geq 0$ is the riskless rate. Then, the price of \mathcal{C} is

$$C(S_0, r, K, \tau) = e^{-r\tau} \mathbb{E}_{\mathbb{Q}} [\max(S_{\tau}^{(\mathbb{Q})} - K, 0)], \quad (15)$$

where $\tau > 0$ denotes the maturity, $K > 0$ is the strike price, and $S_t^{(\mathbb{Q})}$ is the price dynamic of \mathcal{S} on \mathbb{Q} (an equivalent martingale measure of \mathbb{P}). Using MCMM to find the EMM,

$$S_t^{(\mathbb{Q})} = \frac{b_t S_t}{M_{X_t}(1)} = S_0 e^{(r - K_{X_1}(1))t + X_t}, \quad t \in [0, \tau], \quad (16)$$

describes the dynamics of \mathcal{S} on \mathbb{Q} , where $M_{X_t}(v)$ is the MGF of X_t and $K_{X_t}(w) = \ln M_{X_t}(w)$ is the cumulant-generating function of X_t . The chf of the log-price, $\ln S_t^{(\mathbb{Q})}$, is

$$\varphi_{\ln S_t^{(\mathbb{Q})}}(v) = S_0^{iv} \exp\{[iv(r - K_{X_1}(1)) + \psi_{X_1}(v)]t\}, \quad t \in [0, \tau], \quad (17)$$

where $\psi_{X_t}(v)$, $v \in \mathbb{R}$ is the characteristic exponent of X_t .

Carr and Madan (1998) showed how to use the fast Fourier transform (FFT) to value options in the case in which the chf of the log-price of the underlying asset is known analytically. They consider the modified option price $c_a(S_0, r, k, \tau) = e^{ak}C(S_0, r, k, \tau)$, where $k = \ln(K)$, which, for a range of values $a > 0$, guarantees that $c_a(S_0, r, k, \tau)$ is square integrable over $k \in (-\infty, \infty)$. The access point for applying the FFT is their derived relationship

$$C(S_0, r, k, \tau) = \frac{e^{-r\tau - ak}}{\pi} \int_0^{\infty} e^{-ivk} \frac{\varphi_{\ln S_{\tau}^{(\mathbb{Q})}}(v - i(a + 1))}{a^2 + a - v^2 + i(2a + 2)v} dv. \quad (18)$$

Numerical solution of this integral involves two fundamental concerns, an “optimum” value for a and control over the error produced by truncating the integral (18) over a finite domain $[0, v_{\max}]$. Addressing the first of these two concerns, Carr and Madan note that a positive value for a guarantees square-integrability of $c_a(S_0, r, K, \tau)$ over the negative k axis but aggravates square-integrability over the positive k axis. They derive a sufficient condition, $E_{\mathbb{Q}} \left[\left(S_{\tau}^{(\mathbb{Q})} \right)^{a+1} \right] < \infty$ which, combined with the analytic expression for the chf, can be used to determine an upper bound on a . Addressing the second of these concerns, they develop a bound on the error involved in truncating the integration range of (18),

$$v_{\max} > \frac{\exp(-ak) \sqrt{A}}{\pi \epsilon},$$

where ϵ is a desired level of truncation error and \sqrt{A}/v^2 is an upper bound on the magnitude of the integrand in (18).

Constructing the implied volatility surface for call prices requires estimating (18) over a discrete mesh of (k, T) values. Put options can then be valued assuming that put–call parity holds. Implementing a FFT requires numerical discretization of (18) into the form

$$\hat{Z}_p = \sum_{j=1}^M \exp \left[-i \frac{2\pi}{M} (j-1)(p-1) \right] Z_j, \quad k = 1, 2, \dots, M, \quad (19)$$

which the FFT can solve in $O(M \ln_2(M))$ operations. Writing (18) as

$$C(\cdot, \tau, k) = \frac{e^{-r\tau - ak}}{\pi} \Psi(k), \quad \text{where } \Psi(k) = \int_0^{\infty} \exp(-ivk) h(v) dv, \quad (20)$$

discretization of $\Psi(k)$ over a finite range $[0, v_{\max}]$ using the left hand rectangle rule⁸ gives

$$\Psi(k) = \sum_{j=1}^N \exp(-iv_j k) h(v_j) \Delta v, \quad (21)$$

where $v_j = (j-1)\Delta v$, $j = 1, \dots, N$, $v_1 = 0$, $v_N = v_{\max} - \Delta v$. For each fixed value of τ , we discretize $k = \ln(K)$ over a range $[-\bar{k}, \bar{k}]$ with N equally spaced points, $k_p = -\bar{k} + (p-1)\Delta k$, $p = 1, \dots, N$, $\Delta k = 2\bar{k}/N$. On this grid, (21) becomes

$$\Psi(k_p) = \sum_{j=1}^N \exp[-i(j-1)\Delta v(p-1)\Delta k] \exp(i\bar{k}v_j) h(v_j) \Delta v, \quad p = 1, \dots, N, \quad (22)$$

which is identical to (19) with the identifications $\hat{Z}_p = \Psi(k_p)$, $Z_j = \exp(i\bar{k}v_j) h(v_j) \Delta v$, $M = N$, and $2\pi/M = \Delta v \Delta k$. This last identification gives the familiar FFT tradeoff between the span covered in the “space” domain and in the “frequency” domain,

$$v_{\max} \bar{k} = \pi N. \quad (23)$$

In our computations in section 4.1, we used $N = 2^{10} = 1024$.

Carr and Madan (1998) introduced the parameter a to ensure that the call pricing function 15 is square integrable as $K \rightarrow 0$ (i.e., as $k = \ln K \rightarrow -\infty$). They note that a sufficient condition for square integrability is provided by the requirement that $\phi_{\ln(S_t^Q)}(-i(1+a)) \leq \infty$. From 17,

$$\varphi_{\ln S_t^{(Q)}}(-i(1+a)) = S_t^{1+a} \exp\{(1+a)(r_f - K_X(1))T\} \{\exp(K_X(1+a))\}^T \leq \infty. \quad (24)$$

From 8 and 11, note that $\psi(iw) \leq K\psi(w)$ for $w \in \mathbb{R}$. Hence, 24 and $\phi_{\ln(S_t^Q)}(-i(1+a)) \leq \infty$ can be combined as the requirement

$$\exp\{(1+a)(r_f - K_X(1))T\} \{\exp(K_X(1+a))\}^T \leq \infty. \quad (25)$$

To ensure that the cumulant generating function remains real-valued, requirement 25 can be reduced to positive argument requirements for the square root evaluations in 13 for $K_{X_1} \in [1, a]$, where $a \in (0, \infty)$. From 11, under the assumption that $\gamma = 0$, this can be further reduced to the following requirements:

$$h(w) = 1 - \frac{\sigma_3^2 w^2}{\lambda_T} - \frac{2\rho w}{\lambda_T} \geq 0 \quad \text{and} \quad g(w) = 1 - 2\frac{\lambda_U}{\lambda_U} \left(1 - \sqrt{h(w)}\right) \geq 0. \quad (26)$$

Solving the latter equation for $h(w)$ yields

$$h(w) \geq 1 - \frac{\lambda_U}{2\lambda_T} \stackrel{\text{def}}{=} d^2. \quad (27)$$

Combining 27 with the first equation in 26 gives

$$1 - \frac{\sigma_3^2 w^2}{\lambda_T} - 2\frac{\rho w}{\lambda_T} \geq d^2. \quad (28)$$

The quadratic equation has two roots, and Equation 28 is satisfied for $w = 1 + a$ when

$$-\frac{\rho}{\sigma_3^2} - \frac{\sqrt{\rho^2 + \lambda_t \sigma_3^2 (1 - d^2)}}{\sigma_3^2} \leq 1 + a \leq -\frac{\rho}{\sigma_3^2} + \frac{\sqrt{\rho^2 + \lambda_t \sigma_3^2 (1 - d^2)}}{\sigma_3^2} \quad (29)$$

Since a is a non-zero value, it follows that

$$a \leq a_{max} = 1 - \frac{\rho}{\sigma_3^2} + \frac{\sqrt{\rho^2 + \lambda_t \sigma_3^2 (1 - d^2)}}{\sigma_3^2} \quad (30)$$

By utilizing 28, equation 30 can be rewritten as

$$a_{max} = \frac{1}{\sigma_3^2} \sqrt{\rho^2 + \lambda_U \left(1 - \frac{\lambda_U}{4\lambda_T}\right) \sigma_3^2} - \frac{\rho}{\sigma_3^2} - 1. \quad (31)$$

4 Numerical computation

In this section, we illustrate the double subordinated method of sections 2 and 3 and fit the NDIG model to the log-return Bitcoin time series. Figure 1 shows the daily bitcoin price and log-return, r_t time series covering the period from July 19, 2010 to July 28, 2023. The return series consists of 4,026 observations, to which we fit the NDIG model specified by (5)–(8). The NDIG model is characterized by six parameters, $\theta = (\mu_3, \lambda_U, \mu_U, \lambda_T, \mu_T, \sigma_3)$. To further simplify the parameter set $\mu_3, \sigma_3, \gamma, \rho, \lambda_U$, and λ_T , we assume that the subordinator $U(t)$ is used to model the intrinsic time of the return process, while the subordinator $T(t)$ is used to model the return skewness and heavy-tailed behavior. It is reasonable in this model to demand that there be no $\gamma U(t)$ term in 6, i.e., $\gamma = 0$. With this requirement, the first four moments of X become:

$$\begin{aligned}
 E[X] &= \mu_3 + \rho, \\
 Var[X] &= \sigma_3^2 + d\rho^2, \\
 Skew[X] &= \frac{3d\rho(\sigma_3^2 + \rho^2)}{(\sigma_3^2 + d\rho^2)^{3/2}}, \\
 Kurt[X] &= \frac{3\sigma^2 d + 6\rho^2 \sigma (d^2 + 1/\lambda_T^2 + 2/\lambda_U^2) + \frac{15\rho^4}{\lambda_U^3}}{(\sigma_3^2 + d\rho^2)^2},
 \end{aligned} \tag{32}$$

where $\sigma = \rho^2/\lambda_T + \sigma_3^2$, $d = 1/\lambda_T + 1/\lambda_U$.

As there is no analytical expression for the probability density function, we employ the method of moments and the empirical chf to estimate the parameters of the model. We follow Paulson et al. (1975) and Yu (2003) and use the fact that the pdf is the Fourier transform of the chf. So, the five parameters $\mu_3, \sigma_3, \rho, \lambda_U$, and λ_T can be estimated via minimization

$$\begin{aligned}
 &\min_{\mu_3, \sigma_3, \rho, \lambda_T, \lambda_U} \{(\Delta M_1)^2 + (\Delta M_2)^2 + (\Delta M_3)^2 + (\Delta M_4)^2 + (\Delta CF)^2\} \\
 &\text{s.t.} \quad (\Delta M_1)^2 = 1 - \frac{E[X_t]}{E[r_t]}, \\
 &\quad (\Delta M_2)^2 = 1 - \frac{Var[X_t]}{Var[r_t]}, \\
 &\quad (\Delta M_3)^2 = 1 - \frac{Skew[X_t]}{Skew[r_t]}, \\
 &\quad (\Delta M_4)^2 = 1 - \frac{Kurt[X_t]}{Kurt[r_t]}, \\
 &\quad (\Delta CF)^2 = \int_{-\infty}^{\infty} \left(\frac{1}{n} \sum_{j=1}^n e^{ivx_j} - \varphi_{X_t}(v, \theta) \right)^2 dv.
 \end{aligned} \tag{33}$$

where r_t denotes the observed daily bitcoin return time series. The inclusion of the term ΔCF relies on the one-to-one correspondence between the cumulative distribution function

and the characteristic function (since the probability density function is the inverse Fourier transform of the characteristic function). The integral for ΔCF can be estimated using the method described by Yu (2003).

The parameters are estimated by the method of moments and the empirical chf fitting, which is a method as efficient as likelihood-based methods (Yu, 2003).

The resulting parameter estimates are reported in Table 1.

Table 1 NDIG parameter estimates for the bitcoin log returns.

μ_3	λ_U	μ_U	λ_T	μ_T	σ_3	ρ
0.004	0.145	1.00	9.9293	1.00	0.0551	-0.0008

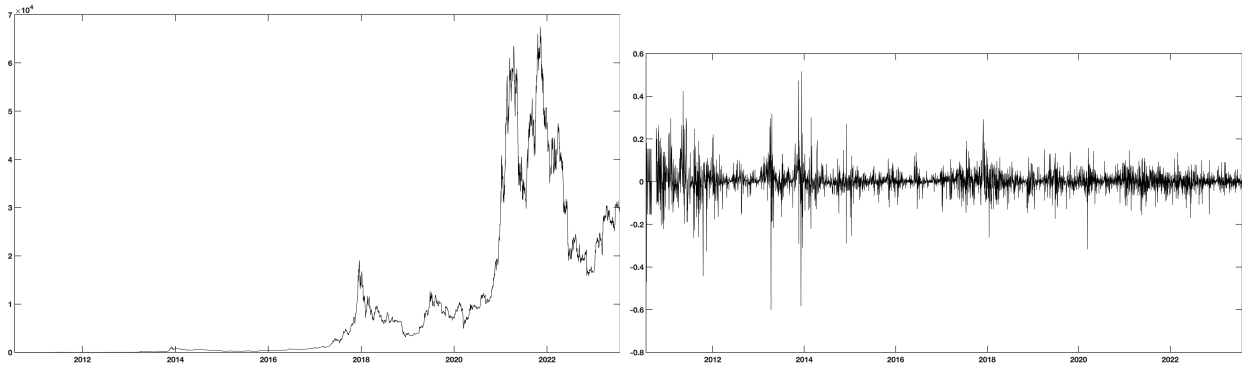


Figure 1 Daily bitcoin data from July 19, 2010 to July 28, 2023.

For comparison, we also fit the normal and the Student’s t distributions to the Bitcoin daily log-return values and estimated the distribution parameters using maximum likelihood. The empirical density, the fitted NDIG model, and the best-fit Student’s t ($df = 1.60$), and normal ($\hat{\mu} = 0.0032$, $\hat{\sigma} = 0.0551$) distribution densities are compared in Figure 2. The results confirm, as was noted in the introduction, that the normal distribution is not well suited for modeling asset returns. The graphs indicate that both the Student’s t and NDIG models match the tails of empirical density rather well, while NDIG matches the skewness in the empirical distribution more evenly than does Student’s t . The low estimate of $df = 1.60$ for the Student’s t distribution implies that even second moments do not exist. Thus, the fat tails of the Student’s t distribution would cause divergence of the BSM integral needed to evaluate price options.

4.1 NDIG Model for European Call Option Pricing

In this section, the NDIG model is used to price a European call option \mathcal{C} with the underlying risky asset \mathcal{S} being the return of Bitcoin. The dynamics of \mathcal{S} under \mathbb{Q} is given by equation

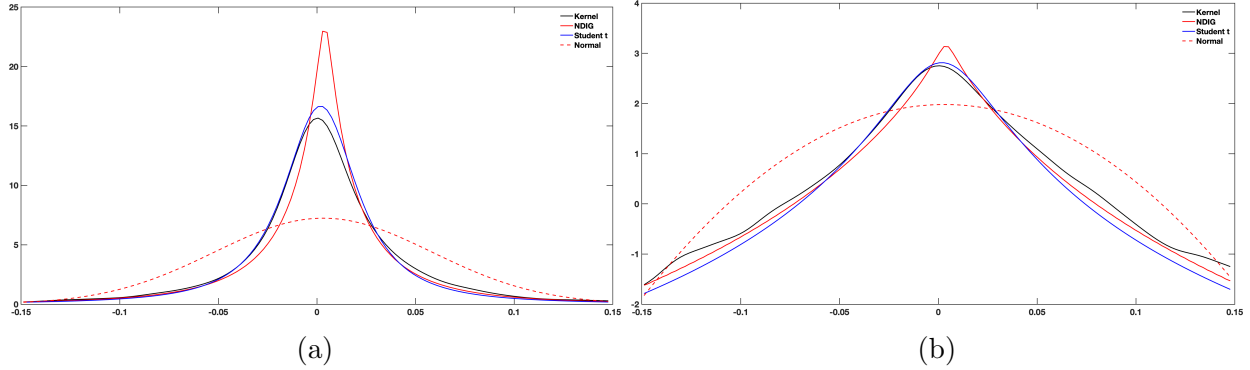


Figure 2 (a) Comparison of normal, Student’s t , and NDIG distribution fits to the kernel density of the bitcoin return. (b) Same plot with the y-axis now in natural log scale.

16, and the characteristic function (CF) of the log-price by equation 17. Option prices for \mathcal{C} are determined by evaluating equation 18 using the Fast Fourier Transform (FFT) for different values of the strike price K and maturity time T . Put option prices are computed using the put-call parity.

We apply the NDIG Lévy model to the pricing of European plain vanilla bitcoin options. Let \mathcal{C} be a European call option where the underlying risky asset, \mathcal{S} , follows the log-price process given in (6). The dynamics of \mathcal{S} on \mathbb{Q} are given by (16) and the chf of the log-price by (17). We evaluate the integral (18) using FFT for a range of strike levels and maturity horizons with the parameter estimates reported in Table 1. When using the global parameter values provided in Table 1, the upper bound of a in 32 is $\lesssim 21.93$.

To ensure that option prices are within acceptable limits, a more stringent determination of the value of $\sigma \in (0, \infty)$ is required. Specifically, for a European call option, the upper and lower bounds on the price are given by $\max(S - Ke^{-r_f T}, 0) \leq C(S_t, T, K) \leq S_T$.²

As noted above, an upper bound value for a and hence choice of a suitable value in performing the integrations via FFT is very dependent on the data set (the price process). When $a > 1$ the call option surface was unstable. We follow Schoutens (2003) and set $a = 0.15$.

Figures 3 (a) and (b) show the resulting prices for call and put options plotted against maturity, τ , and strike price K . Figures (c) and (d) show the implied volatility surfaces, i.e., the market’s view on future volatility, against time to maturity and relative moneyness, defined as K/S , where S is the asset price obtained by the BSM model. Figure 3-(c) investigate the behavior of implied volatility concerning moneyness and time to maturity for both call and put options. It is observed that as moneyness increases, moving towards out-of-the-money values, the implied volatility also increases. Conversely, as moneyness decreases, a distinct pattern emerges, referred to as the “smirk” in the implied volatility curve. Initially, as moneyness decreases and options move in-the-money, implied volatility

²See, e.g., Hull (1993).

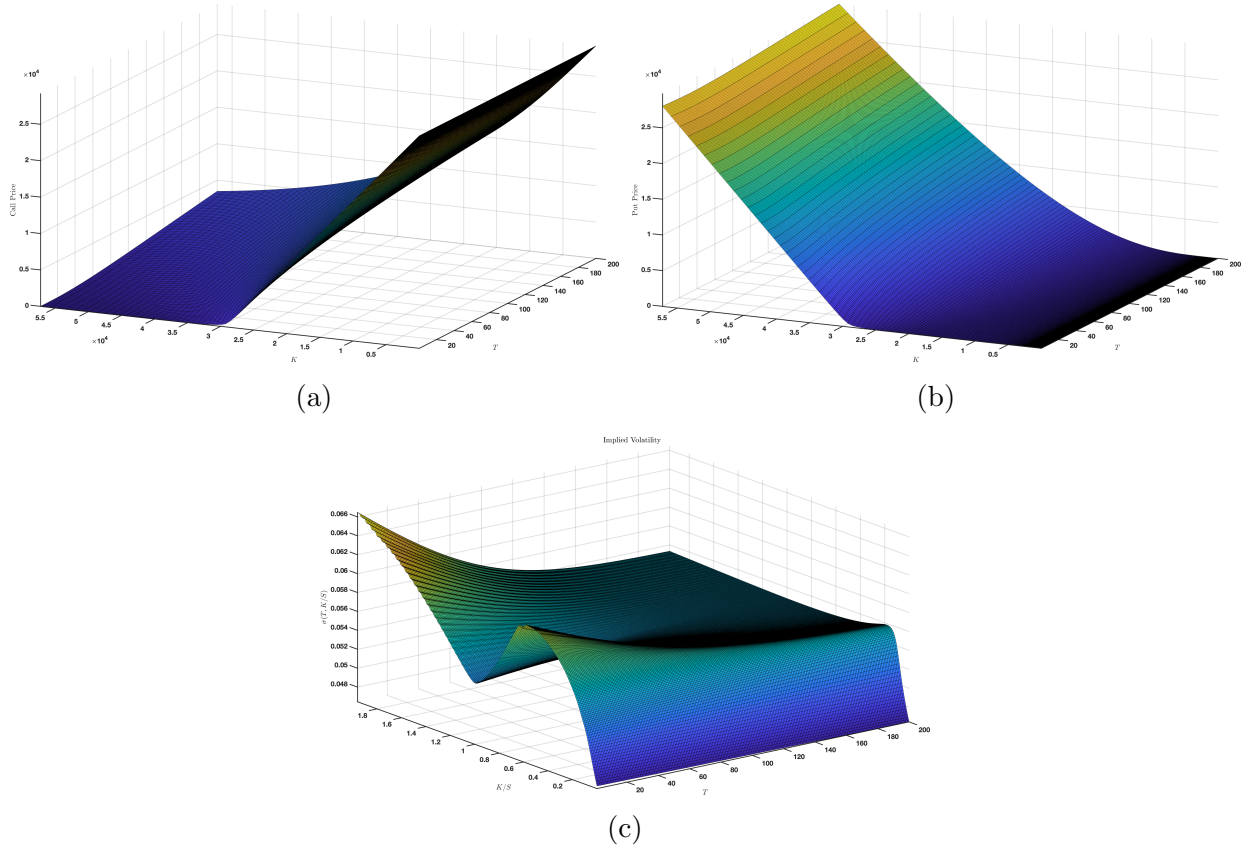


Figure 3 NDIG-based price surfaces for bitcoin (a) call and (b) put options as functions of time to maturity and strike price. (c) Implied volatility surfaces as functions of time to maturity and moneyness.

risers, but subsequently, it starts to decrease for further in-the-money options, eventually approaching near-zero values. As we extend the time to maturity (denoted as τ) of the options, we notice a noteworthy trend. The sensitivity of implied volatility to changes in moneyness diminishes for call options, and this effect appears to converge to a constant level irrespective of the moneyness. In other words, as the options approach their expiration dates, their implied volatility becomes less responsive to changes in moneyness.

5 Bitcoin Volatility Measures

Understanding the volatility of speculative assets is critical for investment decisions. Given that bitcoin is, at least by some, considered to be a potential alternative to fiat money, volatility characteristics are of especial concern. It is, therefore, of interest to understand and adequately model the process that governs the volatility of bitcoin.

Model parameters reflecting the volatility of asset prices are known to vary stochastically

and exhibit clustering. To allow for these phenomena in option pricing, Hull and White (1987) and Heston (1993) suitably randomize the volatility parameter in the Black–Scholes model, where the volatility process is governed by Brownian motion. An alternative strategy was adopted by Carr et al. (2003) based upon ideas by Geman et al. (2001) and Clark (1973). Clark conjectured that price processes are controlled by a random clock, which is a cumulative measure of economic activity, and used transaction volume as a proxy for this measure. Geman et al. suggested the price process must have a jump component; thus the price process can be regarded as Brownian motion subordinated to this random clock. Carr et al. developed this subordinated model using normal inverse Gaussian and variance gamma examples of pure jump Lévy processes. Hurst et al. (1997) considered various subordinated processes to model the leptokurtic characteristics of stock–index returns. In the option pricing literature, Carr and Wu (2004) extended the approach in Carr et al. (2003) by providing an efficient way to allow for correlation between the stock price process and random time changes. Klingler et al. (2013) introduced two new six–parameter processes based on time changing tempered stable distributions and developed an option pricing model based on these processes. Shirvani et al. (2021) introduced the volatility intrinsic time or volatility subordinator model to reflect the heavy–tail phenomena present in asset returns. They studied the question of whether the VIX index is a volatility index that adequately reflects intrinsic time. They showed that this index fails to properly capture the intrinsic time for the SPDR S&P 500. Apparently, the VIX index, as a measure of time change, does not reflect all the information needed to correctly capture the skewness and the fat–tailedness of the S&P 500 index. A model with a suitable volatility subordinator should adequately account for such empirical phenomena.

In this section, we apply three views to analyze bitcoin volatility. The first measures historical realized volatility through sample standard deviation. As noted in the Introduction, this is the method employed in the Bitcoin Volatility Index. The second measures implied (future) volatility in the risk-neutral, derivatives world, \mathbb{Q} , reflecting the views of the option traders. The third measures implied volatility in the real world, \mathbb{P} , reflecting the views of spot traders. We employ an intrinsic time formulation in this latter case. In the following, we empirically compare these three modeling strategies using daily bitcoin data from January 1, 2015 to April 8, 2021.

Historical Volatility. Figure 7 plots the historical volatility series based on measuring average standard deviation on a 1008–day rolling window of bitcoin returns. The historical volatility varies substantially over the sample period, assuming values between 60.69 and 159.62 percent.

Implied Volatility in \mathbb{Q} . Option traders commonly use implied volatility as a proxy for future volatility. The VIX, the index reflecting volatility expectations for the S&P 500 stock index, is based on S&P 500 index options estimated on a real-time basis by the Cboe. The VIX can be regarded as an efficient volatility forecast for the S&P 500 index, provided that option markets are efficient.

The value of the VIX index is

$$VIX = 100 \times \sqrt{W_1\sigma_1^2 + W_2\sigma_2^2} \quad (34)$$

Subscript “1” denotes near-term options while “2” denotes next term options. As SPX options expire on Fridays, depending on the trading day, near-term options have 23 to 30 days until expiration, while next-term options have 31 to 37 days until expiration. The weights W_j ($j = 1, 2$) express these expiration times in a normalized form, accurate to the minute,

$$W_1 = \frac{M_{T_1}}{M_{30}} \left(\frac{M_{T_2} - M_{30}}{M_{T_2} - M_{T_1}} \right), \quad W_2 = \frac{M_{T_2}}{M_{30}} \left(\frac{M_{30} - M_{T_1}}{M_{T_2} - M_{T_1}} \right), \quad (35)$$

where M_j represents the number of minutes until the settlement of the j -th term options, while M_{30} represents the total number of minutes in a 30-day period. As a result, W_1 and W_2 are constrained to the range $0 \leq W_1, W_2 \leq 1$, with the additional requirement that $W_1 + W_2 = 1$. The equation below, provided by Demeterfi et al. (1999), can be used to calculate the near-term and next-term volatilities:

$$\sigma_j^2 = \frac{2e^{r_f T_j}}{T_j} \sum_i \frac{\Delta K_i}{K_i^2} Q(K_i) \frac{1}{T_j} \left(\frac{F_j}{K_{0j}} - 1 \right)^2. \quad (36)$$

Here, T_j is the time to expiration measured in fractions of a year, r_f is the annualized risk-free rate, F_j is the forward index level derived from index option prices, K_{0j} is the first strike price below F_j , K_i is the strike price of the i th out-of-the-money option (a call if $K_i > K_0$, a put if $K_i < K_0$, and both call and put if $K_i = K_0$), ΔK_i is the interval between strike prices, and Q_{K_i} is the midpoint of the bid-ask spread for each option with strike price K_i . For more information on the computation of each of these parameters, refer to the Cboe white paper by CBOE (2019) on VIX.

To calculate a “VIX-like” volatility known as BVIX, the NDIG model is used to compute prices for European put and call options that have between 23 and 37 days to expiration. To compare with the historical volatility, BVIX values are calculated using historical data as follows: for each moving window of length 1008 Bitcoin log-return data,

1. The NDIG model is fitted to the 1008 Bitcoin log-return data (4 years), and the model parameters are estimated using the minimization 33. The resulting parameter values are displayed in Fig. 4. The results depicted unveil discernible patterns among the parameters under investigation. Particularly noteworthy is the conspicuous observation that λ_T displays the least temporal variation, while ρ showcases the highest level of temporal variability. Furthermore, an examination of the estimated values for μ_3 and σ_3 indicates a declining trend leading up to April 2017, followed by a subsequent abrupt change, with relatively minor fluctuations thereafter. Additionally, it is worth noting that the parameter ρ exhibits the smallest magnitude in its estimated value, accompanied by a considerable degree of dispersion or deviation from the mean. These observations are graphically represented in Figure 4, which presents a comparative

visualization of the first four empirical moments derived from the time series depicted in Figure 4 . These moments are contrasted with those computed from the parameters derived via Equation 33. This analysis offers valuable insights into the dynamics and characteristics of the examined parameters.

Fig. 5 compares the first four empirical moments computed from the time series in Fig. 1 and the moments computed from the fitted parameters using 32.

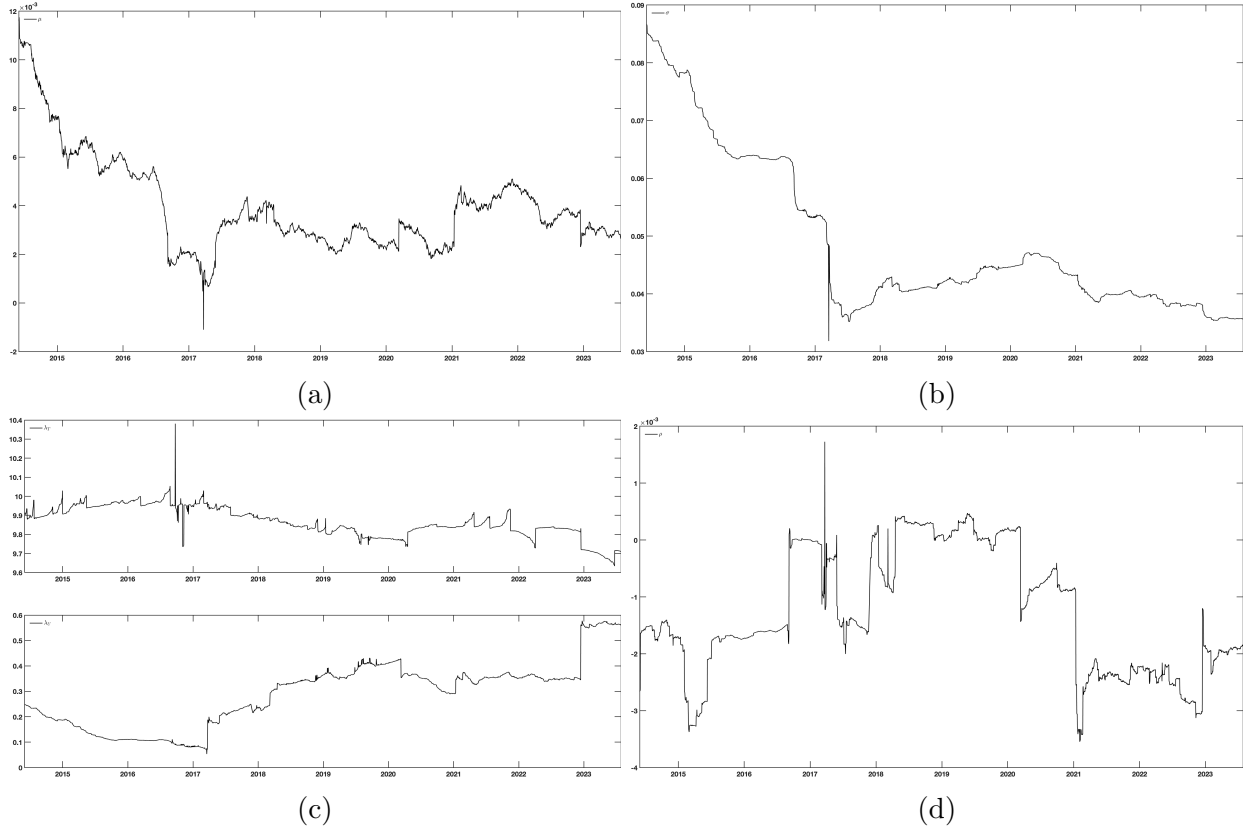


Figure 4 Four-year moving window fits to the parameter values (a) μ_3 , (b) σ_3 , (c) λ_T , and λ_U , and (d) ρ .

2. The dynamics of the Bitcoin price $S_T^{\mathbb{Q}}$ in the risk-neutral world and subsequently, the characteristic function (CF) of the log price $\ln S_T^{\mathbb{Q}}$ are determined using 17.
3. Call option prices with appropriate expiration dates are computed using the FFT formulation 18, and put option prices are computed using put-call parity based on the portfolio spot price $S_T^{\mathbb{Q}}$ for the last date of the moving window. In the context of option price calculations based on 18, the numerical values for the parameters a , a_{\max} , and v_{\max} are determined through the utilization of conditions outlined in ?? and Equation ??, respectively. Choosing too small values for a results in option prices that exceed

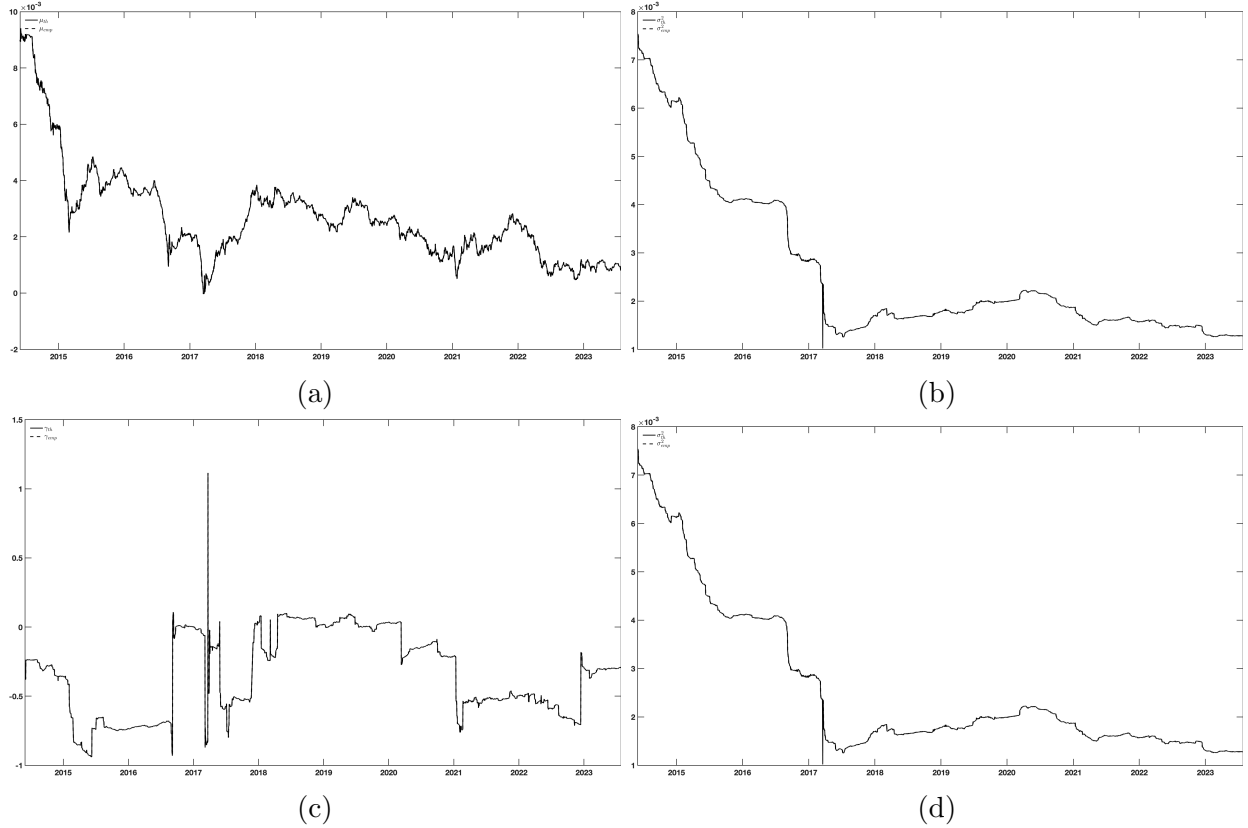


Figure 5 Comparison of the first four empirical (“emp”) moments computed from the return time series and the moments (“th”) computed from the fitted parameters.

the maximum threshold, while choosing a too large produces prices that go below the minimum threshold (and maybe negative). As we discussed, a stricter determination for the value of $a \in [0, a_{max}]$ is based on the requirement that option prices remain within allowed bounds. Fig. 6 shows the computed values for the upper bound a_{max} over period 05/08/2014 through 07/28/2023. For the computations in the remainder of this section, we utilize the smallest possible value, $a = 0.40$.

4. BVIX values are then computed using 34 through 36. As there are no traded options on the Bitcoin data, the following minor modifications were made to the VIX formulation:
 - (a) The risk-free interest rate used is the annualized bond-equivalent (coupon-equivalent) yield for 3-months U.S. treasury bills published for day t .
 - (b) Closing times for option evaluation are at 4 : 00 PM on day t .
 - (c) Options expire on near- and next-term Fridays at 4 : 00 PM.
 - (d) As there is no bid-ask spread in the NDIG option price computations, Q_{K_i} is computed directly as the NDIG option price.

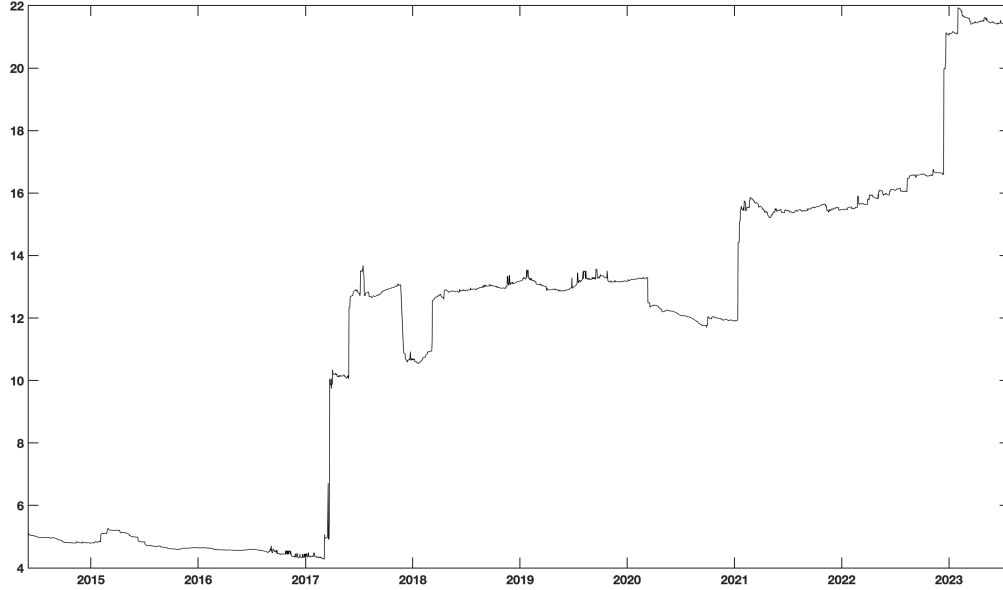


Figure 6 Values for the upper bound a_{max} computed over the period 05/08/2014 through 07/28/2023.

- (e) The range of strike prices considered in the BVIX computation is from $0.75S_t$ to $1.5S_t$, as NDIG computed option prices do not go to zero.

As mentioned in step 4d, since the underlying asset portfolio is not traded, there is no market sentiment setting bid-ask prices for the call and put options used in the BVIX calculation. Therefore, the BVIX volatility directly reflects the NDIG option price computations, and there is no risk premium or market price of risk that is typically captured by the VIX.

Figure 7 shows the values for BVIX. As observed from this figure, BVIX values are higher than STD values. The fact that implied volatility computed from options based upon a risky asset is higher than realized volatility is commonly observed and is referred to as the “volatility risk premium.” An explanation for the volatility risk premium is that option traders allow for the probability of a significant market move. To be compensated for the inherent volatility risk that cannot be hedged away, option sellers charge a premium. Option traders typically view implied volatility as the most reliable approach to volatility forecasting (Jorion, 1995). Figure 7 and a Pearson correlation coefficient of $\rho = 0.48$ between BVIX and historical volatility indicates that implied volatility provides only partial information about future empirical volatility.

To account for the different scales, the historical and BVIX volatility time series can be normalized separately by subtracting the series mean and dividing by the series standard deviation. These normalized plots, as shown in Fig. 8, demonstrate close agreement between the two, with the BVIX volatility displaying a slight daily fluctuation that is not present in the historical volatility. This emphasizes the fact that the sole source of variance in this

numerical example is the daily returns of the underlying risky asset, the Bitcoin data, which is directly quantified by the historical volatility. Since all option prices in this example are calculated using the Carr-Madan formulation and the NDIG model, no additional volatility is introduced to these option prices through, for instance, trader sentiment (bid-ask pricing). Therefore, the BVIX volatility formulation only captures the original asset return volatility.

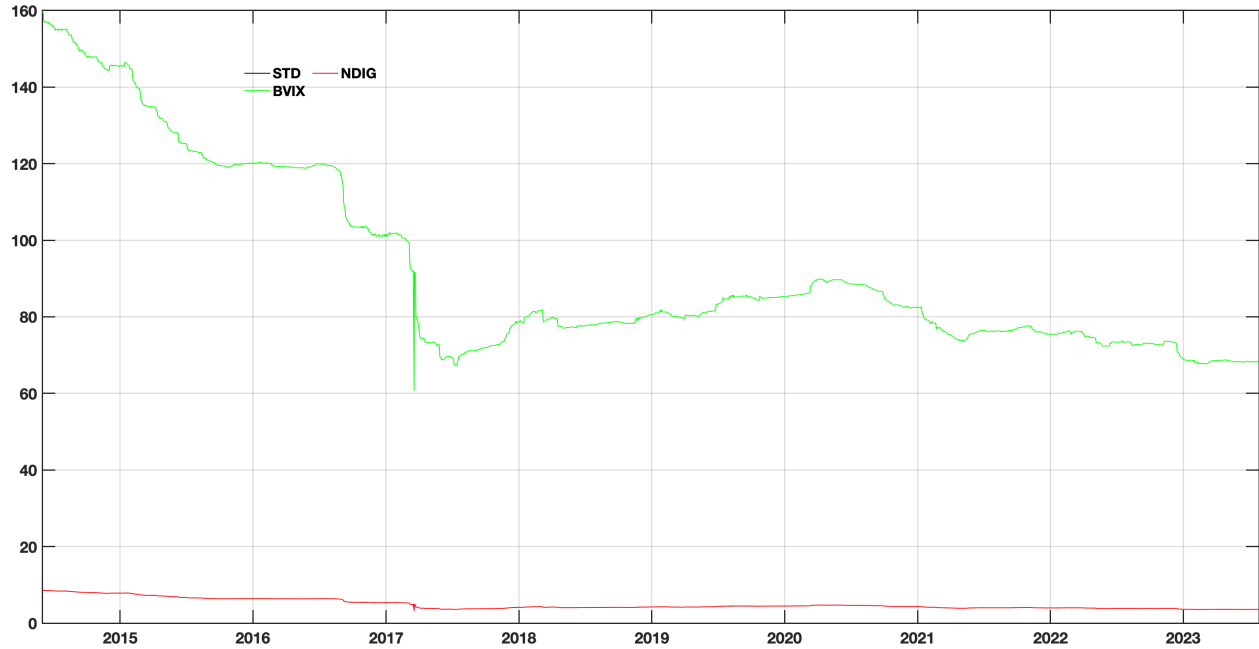


Figure 7 Comparison of bitcoin volatilities computed historically (STD), from option prices (BVIX), and using intrinsic time (NDIG IT). (Y-axis values are in percent.)

Implied Volatility in \mathbb{P} : Intrinsic Time. Mandelbrot and Taylor (1967) coined the term "intrinsic time" in finance to describe how market information is not continuously available, but instead arrives in discrete events occurring at varying intervals. Market orders for assets, for instance, are a prime example of such events, which can differ significantly in both timing and frequency throughout the trading day. These events provide information on asset value (price), and their occurrence, magnitude, and sign characterize intrinsic time. Price change information may also differ in its level of informativeness, with larger changes providing more information than smaller ones, and consecutive price changes of the same sign providing more information than those with opposite signs. Researchers have explored the concept of intrinsic time and applied it to financial time series in various works, including Guillaume et al. (1997), Tsang (2010), and Aloud et al. (2012).

According to the intrinsic time perspective, no information is available between events, and therefore no time has elapsed. An analogy to conceptualize intrinsic time is to imagine an analog clock's seconds-hand that ticks intermittently and randomly, varying in volume

with each tick. Time only moves forward when the hand advances, and the tick’s volume represents the amount of information conveyed.

By utilizing the double subordinated method, a novel measure of volatility can be derived under the \mathcal{P} measure. From (5), we view X_t as the process governing the intrinsic time of the double subordinated price process. From (32) with $\gamma = 0$, the standard deviation (i.e. the volatility) of the unit increment of X_t , when X_t follows a NDIG log-price process, is given by

$$\text{Vol}(X_1) \equiv \sqrt{\text{Var}(X_1)} = \sigma_3^2 + \rho^2 \left(\frac{1}{\lambda_T} + \frac{1}{\lambda_U} \right) \quad (37)$$

where λ_T , λ_U , and σ_3 are model parameters as defined in Table 1. We can refer to the volatility $\sqrt{\text{Var}(X_1)}$ as the NDIG volatility, which takes into account both the Brownian motion (Gaussian) and Lévy subordinator components of the model. However, it is important to note that this measure differs from other measures of volatility in the literature.

To derive the intrinsic time for the bitcoin log-price process, we compute rolling NDIG parameter estimates from the recent six years of daily data, using overlapping windows with a length of 1008 days. We use (37) to derive the annualized volatility implied by the NDIG model. The volatility computed by the NDIG intrinsic time model (NDIG IT) is also shown in Figure 7.

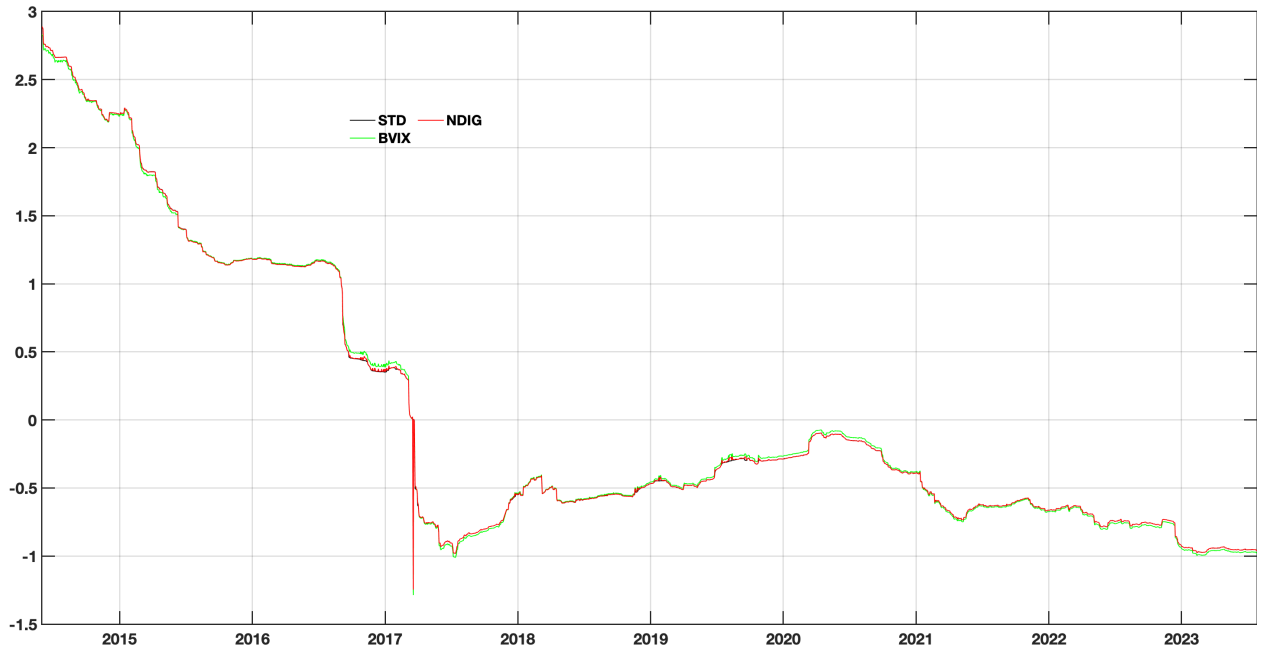


Figure 8 Normalized (mean subtracted, standard deviation scaled) versions of the bitcoin volatility series in Figure 7.

Examination of all three volatility plots reveals substantial similarity between the patterns of NDIG intrinsic time and historical volatility, confirming that (37) captures realistic

bitcoin dispersion patterns. We have addressed above the observed differences between the BVIX implied volatility and historical volatility. We note that the NDIG IT volatility predictions are consistently larger than historical, but otherwise demonstrate very strong synchronicity. Normalized⁹ versions of the three series are plotted in Figure 8. The normalized NDIG IT and STD time series are now virtually identical, indicating an almost perfect linear correlation between the two. The BVIX variant is less synchronous but still co-moves to a certain degree, with a strong pattern of anticipating cycles of high volatility.

Table 2 p -values from augmented Dickey-Fuller (ADF), KPSS and Johansen tests

Test	BVIX	NDIG IT	STD	Test	$r = 0$	$r = 1$
ADF	0.009	0.007	0.001	Johansen	0.001	0.001
KPSS	0.010	0.010	0.010			

Cointegration analysis is one approach to assess whether or not there are significant deviations in co-movement among time series. To apply cointegration, we first check whether each volatility series is integrated. The results of both the augmented Dickey-Fuller and KPSS tests (Kwiatkowski et al., 1992) shown in Table 2 support the hypothesis that each series is integrated of order one (has a unit root). Performing a Johansen test (Johansen, 1988) involving all three time series (Table 2) indicates a cointegrating relationship of orders 1 and 2 among the three time series.

Taken together, the results from Figure 8 and Table 2 show that the dynamic NDIG IT model, which is consistent with dynamic asset pricing theory and has predictive capabilities, provides very good agreement when applied “in-sample”. The implied volatility model, BVIX, which is also dynamic and predictive, has poorer agreement with the in-sample data. The pattern of BVIX often, though not always, anticipating cycles of high volatility may speak to option traders’ heightened sensitivity to potential increases in market volatility.

Finally, we investigate the question of whether there is long-range dependency (LRD) in bitcoin volatility, as has been found in stock volatility (see, for example, Asai et al., 2012). We fit a fractionally integrated autoregressive conditional heteroskedastic (FIGARCH) model to investigate both short- and long-range dependency in the bitcoin variance series. Specifically, we fit an AR(1)-FIGARCH(1, d ,1)¹⁰ with Student’s t innovations. Fractional integration in the GARCH part, i.e., $d > 0$, indicates LRD in volatility and non-stationarity. For $d < 0$ we have anti-persistence and short-range memory. The AR(1)-FIGARCH(1, d ,1) model parameters are estimated in a rolling fashion using a window of 252-day window. Figure 9 plots the sequence of d estimates in the conditional heteroskedastic equation for the variance. The estimates fall almost exclusively in the interval (0.8, 1.0), indicating non-stationarity and the presence of LRD in bitcoin volatility. This implies that volatility measures derived from historical data can be used to determine bitcoin volatility—a finding that also follows from Figure 8, showing that the (normalized) historical standard deviation and NDIG intrinsic time move closely together.

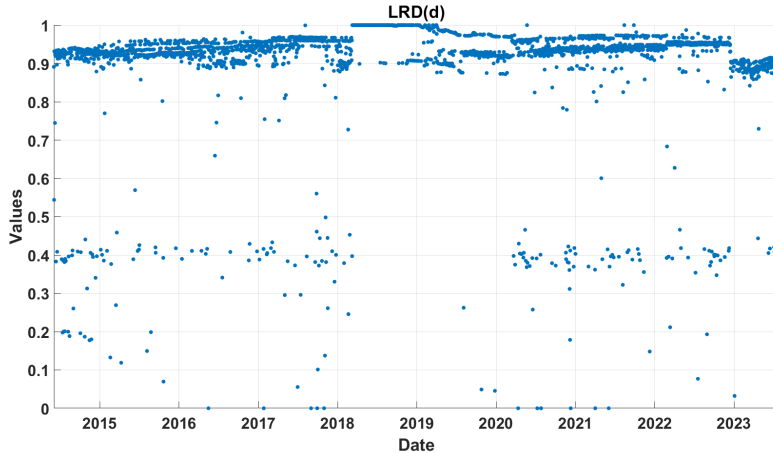


Figure 9 Time-varying LRD (d) in the bitcoin volatility log-return process.

6 Discussion

Dealing with heavy-tailed asset returns remains a challenge in theoretical and empirical finance. Implicit in our approach is that there is a relationship between arrival times of financial news, the “intrinsic time” of finance, and price volatility for an asset, and particularly for bitcoin, whose volatility is especially pronounced. As noted by Clark (1973), “The different evolution of price series on different days is due to the fact that information is available to traders at a varying rate. On days when no new information is available, trading is slow, and the price process evolves slowly. On days when new information violates old expectations, trading is brisk, and the price process evolves much faster.” Our analysis is based on the assumption that information (whether unexpected or reinforcing) arrives at a rate that defines an “intrinsic” or “operational” time scale. Whether this intrinsic time is measured in rate (ticks) or volumes of transactions, or another proxy is irrelevant; we take as a stylized fact that the intrinsic time distribution of information arrival is skewed and extremely heavy tailed. (See, for example, ? on the microstructure of the time between successive transactions.)

The philosophy behind our approach is therefore as follows. The log-price process is additive Brownian motion (Equation (2)), but the time variable that drives the Brownian motion is not the physical time t as suggested by (2), but is an intrinsic or operational time. We utilize subordinated Lévy processes to mimic a relationship between intrinsic time and price processes observed in physical time. Unfortunately, as has been demonstrated by ?, a single level of subordination (equation (4)) is insufficient to capture both the stylized facts of the operational time scale and the stylized facts (skewness, heavy-tails, clustering) observed in asset returns. In this paper we show that, for a very volatile asset, a doubly subordinated process (equation (6)) using a normal inverse Gaussian process at each level of subordination is capable of capturing (Figure 2) the skewness and heavy-tailed behavior of the asset’s return process in physical time, and is, presumably also accounting for the

heavy-tailed distribution of the underlying operational time.

By extending our double subordination approach to option pricing, we are able to show convincingly that not only does the double subordination model capture the distributional properties of the price dynamics, it very accurately captures (Figure 7) the trend of the historical (in-sample) bitcoin volatility (as measured by historical standard deviation). Further, Figure 8, demonstrates that we can derive the correct linear scaling to be applied to the double subordinated model to capture actual (in-sample) volatility.

NOTES

¹ See <https://www.buybitcoinworldwide.com/volatility-index/>.

² The CRIX index captures the performance of a basket of ten leading cryptocurrencies that are listed on well-known, transparent exchanges and meet certain liquidity and market capitalization requirements. S&P Global, through its S&P Dow Jones Indices division, has also introduced an index, the S&P Cryptocurrency MegaCap Index (see S&P-Dow-Jones-Indices, 2021), which is comprised of the S&P Bitcoin Index and the S&P Ethereum Index.

³ See Bochner (1995), Sato (1999) and Schoutens (2003).

⁴ For a further discussion of the use of subordinators in financial modeling, see Sato (1999) and Schoutens (2003).

⁵ We use \sim to denote “equal in distribution” or “equal in probability law.”

⁶ As reported by *Bloomberg Professional Services*, access date 04-08-2021.

⁷ See Duffie (2010, Chapter 6).

⁸ This can be adapted in a straightforward manner for higher order integration rules.

⁹ Specifically, the data set $X = \{x_1, x_2, \dots, x_n\}$ is normalized as $\bar{X} = \{\bar{x}_1, \bar{x}_2, \dots, \bar{x}_n\}$, with $\bar{x}_i = (x_i - x_{\min})/s_x$, where $x_{\min} = \min_{i=1}^n(x_i)$ and s_x is the standard error of the data set.

¹⁰ Cf. Granger and Joyeux (1980), Engle (1982) and Bollerslev and Mikkelsen (1996).

References

- Alexander, C. and A. Imeraj (2021). The bitcoin vix and its variance risk premium. *The Journal of Alternative Investments* 23(4), 84–109.
- Allen, D. E., M. McAleer, and M. Scharth (2011). Monte carlo option pricing with asymmetric realized volatility dynamics. *Mathematics and Computers in Simulation* 81(7), 1247–1256.
- Aloud, M., E. Tsang, R. Olsen, and A. Dupuis (2012). A directional-change event approach for studying financial time series. *Economics* 6(1), 20120036.
- Asai, M., M. McAleer, and M. C. Medeiros (2012). Asymmetry and long memory in volatility modeling. *Journal of Financial Econometrics* 10(3), 495–512.
- Black, F. and M. Scholes (1973). The pricing of options and corporate liabilities. *Journal of Political Economy* 81, 637–654.
- Bochner, S. (1995). *Harmonic Analysis and the Theory of Probability*. Berkeley, CA: University of California Press.
- Bollerslev, T. and H. O. Mikkelsen (1996). Modeling and pricing long memory in stock market volatility. *Journal of econometrics* 73(1), 151–184.
- Carr, P., H. Geman, D. B. Madan, and M. Yor (2003). Stochastic volatility for lévy processes. *Mathematical finance* 13(3), 345–382.
- Carr, P. and D. Madan (1998). Option valuation using the fast fourier transform. *Journal of Computational Finance* 2, 61–73.
- Cassidy, D. T., M. J. Hamp, and R. Ouyed (2010). Pricing european options with a log student’s t-distribution: A gosset formula. *Physica A: Statistical Mechanics and its Applications* 389(24), 5736–5748.
- CBOE, V. (2019). White paper cboe volatility index.
- Clark, P. (1973). A subordinated stochastic process model with fixed variance for speculative prices. *Econometrica* 41, 135–156.
- Demeterfi, K., E. Derman, M. Kamal, and J. Zou (1999). A guide to volatility and variance swaps. *The Journal of Derivatives* 6(4), 9–32.
- Duffie, D. (2010). *Dynamic asset pricing theory*. Princeton University Press.
- Engle, R. F. (1982). Autoregressive conditional heteroscedasticity with estimates of the variance of united kingdom inflation. *Econometrica: Journal of the econometric society*, 987–1007.

- Geman, H., D. B. Madan, and M. Yor (2001). Time changes for lévy processes. *Mathematical Finance* 11(1), 79–96.
- Granger, C. W. and R. Joyeux (1980). An introduction to long-memory time series models and fractional differencing. *Journal of time series analysis* 1(1), 15–29.
- Guillaume, D. M., M. M. Dacorogna, R. R. Davé, U. A. Müller, R. B. Olsen, and O. V. Pictet (1997). From the bird’s eye to the microscope: A survey of new stylized facts of the intra-daily foreign exchange markets. *Finance and stochastics* 1, 95–129.
- Heston, S. L. (1993). A closed-form solution for options with stochastic volatility with applications to bond and currency options. *The review of financial studies* 6(2), 327–343.
- Hull, J. (1993). *Options, futures, and other derivative securities*, Volume 7. Prentice Hall Englewood Cliffs, NJ.
- Hull, J. and A. White (1987). The pricing of options on assets with stochastic volatilities. *The journal of finance* 42(2), 281–300.
- Hurst, S. R., E. Platen, and S. T. Rachev (1997). Subordinated market index models: A comparison. *Financial Engineering and the Japanese Markets* 4(2), 97–124.
- Johansen, S. (1988). Statistical analysis of cointegration vectors. *Journal of economic dynamics and control* 12(2-3), 231–254.
- Jorion, P. (1995). Predicting volatility in the foreign exchange market. *The Journal of Finance* 50(2), 507–528.
- Kim, A., S. Trimborn, and W. K. Härdle (2019). Vcrix-a volatility index for cryptocurrencies. *Available at SSRN 3480348*.
- Klingler, S., Y. S. Kim, S. T. Rachev, and F. J. Fabozzi (2013). Option pricing with time-changed lévy processes. *Applied financial economics* 23(15), 1231–1238.
- Kwiatkowski, D., P. C. Phillips, P. Schmidt, and Y. Shin (1992). Testing the null hypothesis of stationarity against the alternative of a unit root: How sure are we that economic time series have a unit root? *Journal of econometrics* 54(1-3), 159–178.
- Lindquist, W. B., S. T. Rachev, Y. Hu, and A. Shirvani (2022). *Option Pricing*, pp. 197–226. Cham: Springer International Publishing.
- Lundtofte, F. and A. Wilhelmsson (2013). Risk premia: Exact solutions vs. log-linear approximations. *Journal of Banking & Finance* 37, 4256–4264.
- Mandelbrot, B. B. and H. M. Taylor (1967). On the distribution of stock price differences. *Journal of Operations Research* 15, 1057–1062.

- Merton, R. C. (1973). Theory of rational option pricing. *Bell Journal of Economics and Management Science, The RAND Corporation* 6, 141–183.
- Näf, J., M. S. Paoletta, and P. Polak (2019). Heterogeneous tail generalized comfot modeling via cholesky decomposition. *Journal of Multivariate Analysis* 172, 84–106.
- Osterrieder, J. (2016). The statistics of bitcoin and cryptocurrencies. *Available at SSRN 2872158*.
- Paulson, A. S., E. W. Holcomb, and R. A. Leitch (1975). The estimation of the parameters of the stable laws. *Biometrika* 62, 163–170.
- Sato, K.-I. (1999). *Lèvy Processes and Infinitely Divisible Distributions*. Cambridge: Cambridge studies in advanced mathematics.
- Schoutens, W. (2003). *Lévy Processes in Finance: Pricing Financial Derivatives*. Hoboken, NJ: John Wiley & Sons.
- Shirvani, A., S. T. Rachev, and F. J. Fabozzi (2021). Multiple subordinated modeling of asset returns: Implications for option pricing. *Econometric Reviews* 40(3), 290–319.
- Shirvani, A., S. V. Stoyanov, F. J. Fabozzi, and S. T. Rachev (2021). Equity premium puzzle or faulty economic modelling? *Review of Quantitative Finance and Accounting* 56, 1329–1342.
- S&P-Dow-Jones-Indices (2021). S&P cryptocurrency index series. Available at <https://www.spglobal.com/spdji/en/education/article/faq-sp-cryptocurrency-index-series/#:~:text=As%20of%20May%203%2C%202021,of%20the%20digital%20asset%20Ethereum>.
- T3I-Pty-Ltd. (2019). Indices bitvol. Available at <https://www.buybitcoinworldwide.com/volatility-index/>.
- Tsang, E. (2010). Directional changes, definitions. *Working Paper WP050–10 Centre for Computational Finance and Economic Agents (CCFEA), University of Essex Revised 1, Tech. Rep.*
- Venter, P. J. and E. Maré (2020). Garch generated volatility indices of bitcoin and crix. *Journal of Risk and Financial Management* 13(6), 121.
- Yao, L., G. Yang, and X. Yang (2011). A note on the mean correcting martingale measure for geometric lévy processes. *Applied Mathematics Letters* 24(5), 593–597.
- Yu, J. (2003). Empirical characteristic function estimation and its applications. *Econometric Reviews* 23, 93–123.